ARL-TR-9136 ● JAN 2021

Worm-Drive Actuator Prototype for a Fin-Controlled Projectile

by Joshua T Bryson and Ilmars Celmins

NOTICES

Disclaimers

The findings in this report are not to be construed as an official Department of the Army position unless so designated by other authorized documents.

Citation of manufacturer's or trade names does not constitute an official endorsement or approval of the use thereof.

Destroy this report when it is no longer needed. Do not return it to the originator.

ARL-TR-9136 ● JAN 2021

Worm-Drive Actuator Prototype for a Fin-Controlled Projectile

Joshua T Bryson and Ilmars Celmins
Weapons and Materials Research Directorate,
DEVCOM Army Research Laboratory

REPORT DOCUMENTATION PAGE

Form Approved
OMB No. 0704-0188

1. REPORT DATE *(DD-MM-YYYY)*	**2. REPORT TYPE**	**3. DATES COVERED (From - To)**
January 2021	Technical Report	1 October–14 November 2020

4. TITLE AND SUBTITLE
Worm-Drive Actuator Prototype for a Fin-Controlled Projectile

5a. CONTRACT NUMBER

5b. GRANT NUMBER

5c. PROGRAM ELEMENT NUMBER

6. AUTHOR(S)
Joshua T Bryson and Ilmars Celmins

5d. PROJECT NUMBER

5e. TASK NUMBER

5f. WORK UNIT NUMBER

7. PERFORMING ORGANIZATION NAME(S) AND ADDRESS(ES)
DEVCOM Army Research Laboratory
ATTN: FCDD-RLW-LE
Aberdeen Proving Ground, MD 21005-5067

8. PERFORMING ORGANIZATION REPORT NUMBER
ARL-TR-9136

9. SPONSORING/MONITORING AGENCY NAME(S) AND ADDRESS(ES)

10. SPONSOR/MONITOR'S ACRONYM(S)

11. SPONSOR/MONITOR'S REPORT NUMBER(S)

12. DISTRIBUTION/AVAILABILITY STATEMENT
Approved for public release; distribution is unlimited.

13. SUPPLEMENTARY NOTES
ORCID ID: Joshua T Bryson, 0000-0002-0753-6823

14. ABSTRACT
This report presents a prototype actuator design for a fin-controlled projectile. The mechanical design is presented, followed by a description of the control-system architecture. The tuned control-system parameters are given along with results from bench-level experiments demonstrating the closed-loop dynamic response. Models are fit to the experiment response data to characterize the dynamic behavior, and the actuator is shown to meet bandwidth requirements.

15. SUBJECT TERMS
control actuation, fin control, guided munition, long-range precision fires, actuator design, actuator dynamics

16. SECURITY CLASSIFICATION OF:			**17. LIMITATION OF ABSTRACT**	**18. NUMBER OF PAGES**	**19a. NAME OF RESPONSIBLE PERSON**
a. REPORT	**b. ABSTRACT**	**c. THIS PAGE**			Joshua T Bryson
Unclassified	Unclassified	Unclassified	UU	22	**19b. TELEPHONE NUMBER (Include area code)** (410) 306-1939

Standard Form 298 (Rev. 8/98)
Prescribed by ANSI Std. Z39.18

Contents

List of Figures

List of Tables

1. Introduction

The Army is prioritizing research into long-range precision fires (LRPFs) technologies as part of the multi-domain operation concept for competing in a contested environment against a near-peer adversary. Supporting this goal, the US Army Combat Capabilities Development Command Army Research Laboratory has established an Essential Research Program dedicated to the development and maturation of LRPF-relevant technologies. Under this research program, DEVCOM Army Research Laboratory is developing a Laboratory Technology Vehicle (LTV) projectile to serve as a modular, flexible, in-house testbed to more easily/rapidly conduct free-flight experiments with component-level LRPF research products.

The goals for this control actuation system (CAS) research are twofold: 1) provide a functional CAS for the LTV to enable full-system flight experiments in the near term, and 2) establish a benchmark understanding of the current state of the art for CAS technologies to understand the current gaps and limitations to focus future research on transformational technologies enabling high-speed, maneuverable munitions for the Army.

Recent research and analysis focused on the LTV airframe identified actuator requirements derived from the airframe dynamics and the margins of the flight control system.[1] This work identified the design goal for the closed-loop actuator bandwidth, ω_{BW}, of at least 300 rad/s to avoid degradation of flight control performance. Additional requirements for output torque to overcome anticipated aerodynamic loading on the control surfaces were also identified through aerodynamic modeling and flight dynamics analysis.[1,2] However, this work only focuses on the performance of the unloaded actuator as a first step enabling future work with the closed-loop actuator under simulated flight loadings.

This report is organized as follows. An overview of the LTV airframe is presented along with the mechanical design of the actuator. A physics-based actuator model is presented, and the current and position control architectures are introduced. Experiment results showing the closed-loop actuator response are shown along with model fits. Finally, a second-order ordinary differential equation (ODE) is fit to the experiment and the performance is compared with the previously identified bandwidth requirements.

2. Airframe Overview

An overview of the LTV flight body is shown in Fig. 1. The body diameter is 105 mm and the overall length is 1050 mm. The nose has a 30% ogive as a tradeoff between drag reduction and payload volume. The projectile is launched from an 8-inch smoothbore gun using a pusher sabot. There are four low-aspect-ratio fins arrayed symmetrically around the body to provide lift and stability.

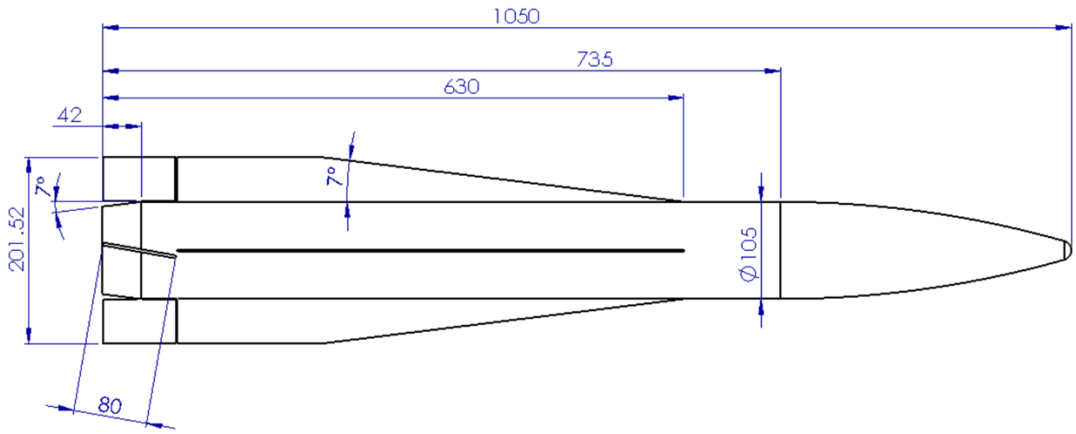

Fig. 1 Overview of the LTV flight body

Control is provided using 80-mm chord trailing-edge flaps on the fins, which are pivoted at the mid-chord location. The Quad Tail Control Actuation System (QT-CAS) module was designed to fit in the rear of the LTV and actuates four trailing-edge fin flaps. Figure 2 is the solid model of the LTV, showing how the QT-CAS module fits into the LTV projectile.

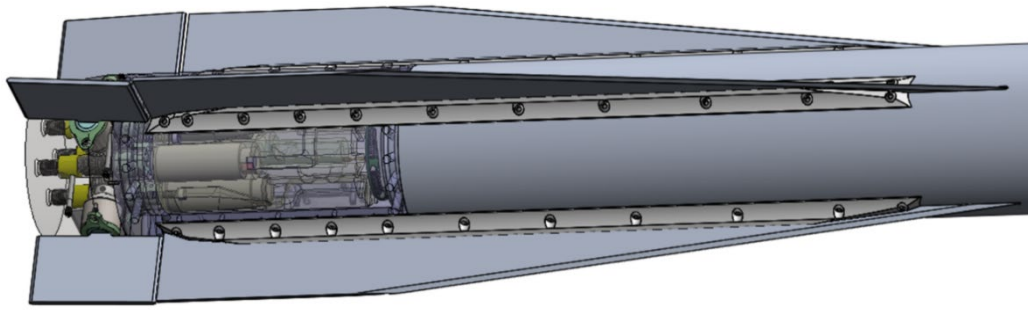

Fig. 2 CAS inside the LTV projectile body

3. Actuator Mechanical Design

The basic CAS design concept is to have four brushless motors, each driving a control surface through a worm-gear drive train. The gear ratio was chosen to be 20:1 based on initial estimates of motor torque and speed, plus anticipated flap

torque loading and required actuation response. Figure 3 shows the motor and worm-gear mechanism in more detail.

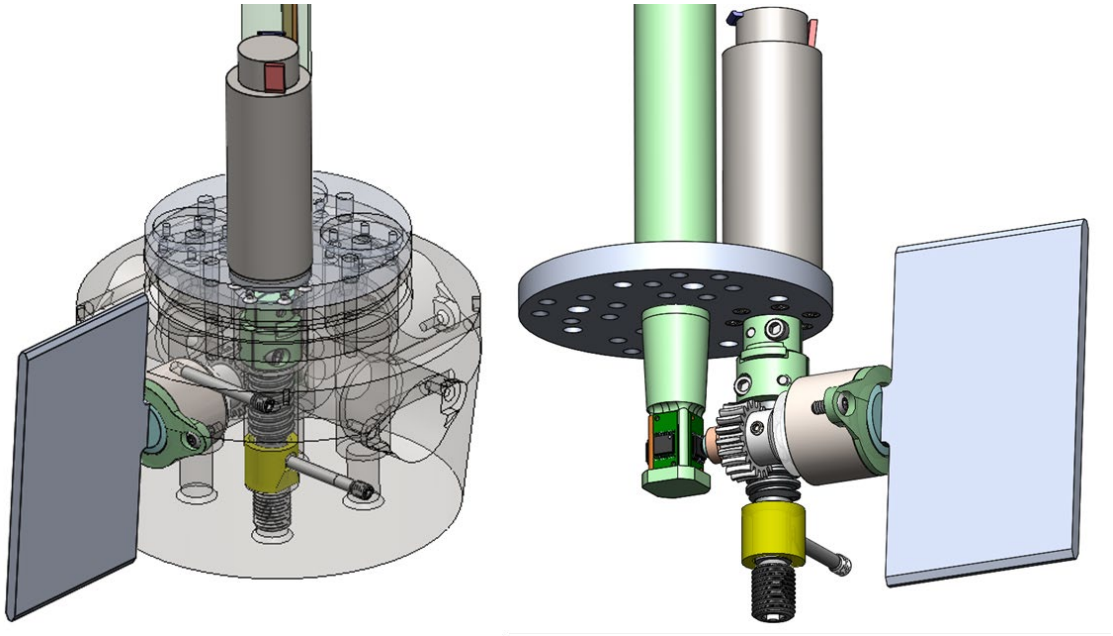

Fig. 3 QT-CAS motor and gear details for a single axis

The motor chosen to actuate the fin is a Maxon EC-4pole 22-mm 90-W brushless motor with a 512-count-per-turn ENX 16 EASY encoder on the motor shaft for feedback. The gears were from Stock Drive Products/Sterling Instrument: a 20-tooth gear (part number [PN] A 1P 6MYK08R020) and single-lead worm (PN A 1Y 5MYK08RB). An additional magnetic encoder is mounted at the output shaft to directly read the flap angle (AMS AS5048).

A bench test version of a single axis of the CAS was designed and assembled to facilitate performance characterization and iterate the initial design, as shown in Fig. 4. An aluminum block was used to mount the motor, worm-gear assembly, and the output shaft in exactly the same manner as it is held in the projectile. A steel inertia simulant (not shown for clarity) is attached to the output shaft to emulate the control-surface inertia for dynamic testing. Thus, the friction, gear engagement, and inertias of the moving parts match those of the final QT-CAS module installed in the projectile as closely as possible.

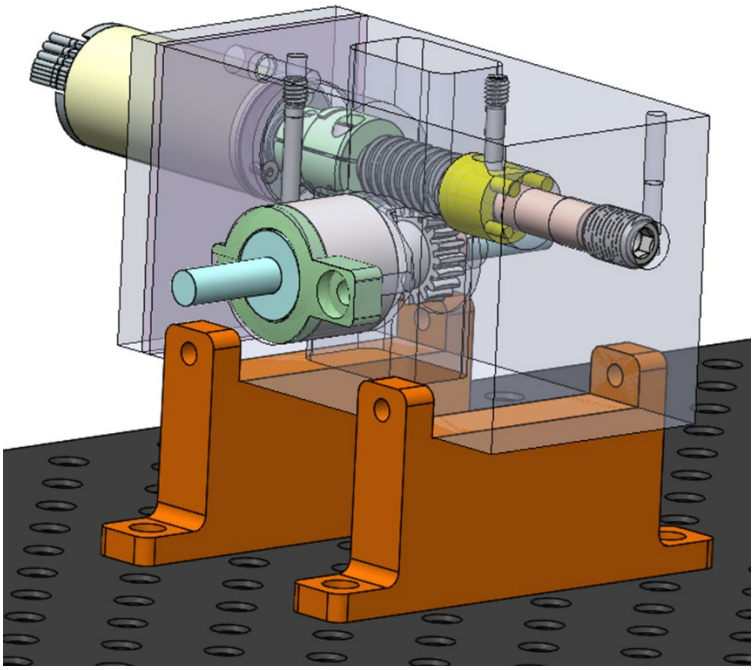

Fig. 4 Bench test version of a single axis of the QT-CAS

4. Actuator Model and Control Architecture

The brushless motor and mechanical drive train are modeled using the simplified dynamic model shown in Fig. 5, which models the translation of a voltage command to the motor into drive outputs such as current, position, angular velocity and acceleration, and output torque.[3] The model is defined using the motor characteristic parameters of winding resistance, R, winding inductance, L, motor torque constant, K_m, electrical constant, K_e, rotational inertia, J, and viscous friction, μ_v.

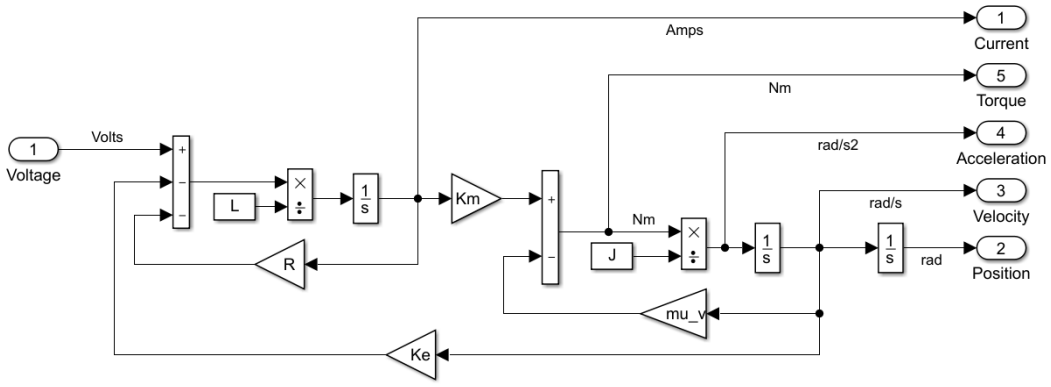

Fig. 5 Simple model of the actuator electric motor and drivetrain

The controller used to provide closed-loop position control of the actuator in this series of bench testing contains an inner proportional–integral (PI) current control loop and an outer proportional–integral-derivative (PID) position control loop. The current controller varies the applied motor voltage to maintain a desired electrical current through the motor. The PI current control architecture is given in Fig. 6, with proportional gain, K_p, and integral gain, K_i. An anti-windup feature is included on the integral term to prevent the integrated error from increasing if the voltage command is above the saturation level of the power supply or motor control electronics. The time delay for the current control loop is 0.06 ms.[3]

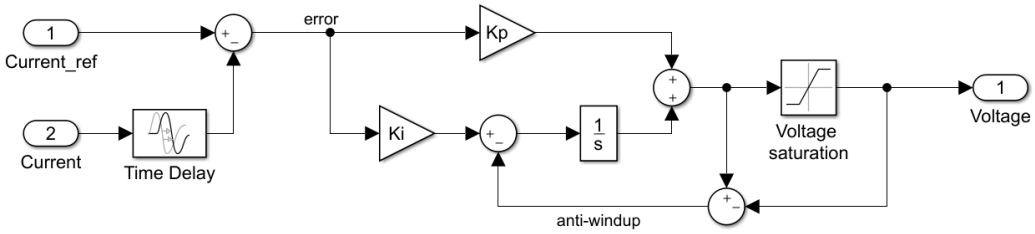

Fig. 6 Architecture of the PI current controller

The position controller varies the motor current to achieve a desired position of the motor–drivetrain assembly. The PID position control architecture is given in Fig. 7, with K_p, K_i, and filtered derivative gain, D, given by the transfer function

$$D = \frac{K_p \mathbf{s}}{\frac{K_d}{10K_p}\mathbf{s} + 1}$$

The PID position controller has optional feed-forward inputs for velocity, FF_v, and acceleration, FF_a, for use with a trajectory planner to improve the system dynamic response in the presence of high friction or inertia. These desired velocity and acceleration feedforward terms are multiplied by the FF_V and FF_a gains, respectively. As with the current controller, an anti-windup feature is included on the integral term to prevent buildup of the integration error when the current command is above the saturation level. The time delay for the position control loop is 0.4 ms.[3]

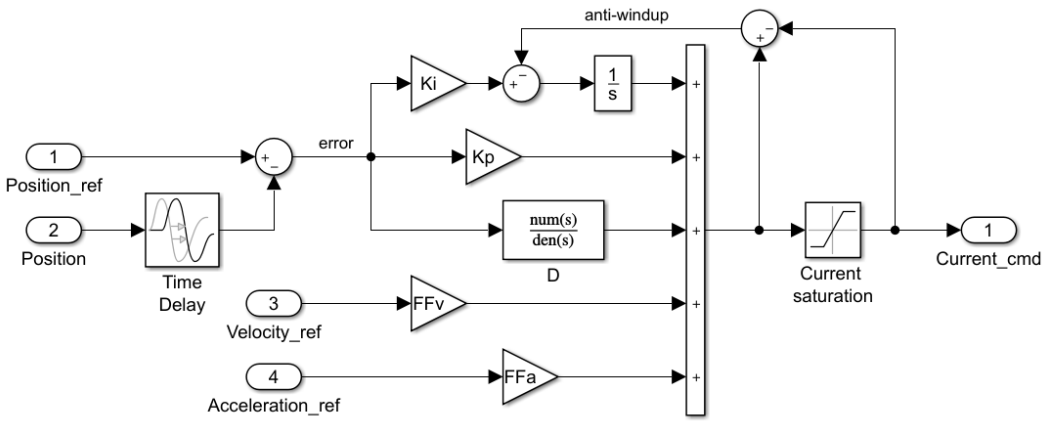

Fig. 7 Architecture of the PID position controller with optional feed-forward inputs for velocity and acceleration

Combining the plant model from Fig. 5 with the current and position controllers from Figs. 6 and 7 gives a model of the closed-loop actuator, shown in Fig. 8. For the performance testing in this work, the desired position command is the only input to the position controller, with the FF_v and FF_a commands held to zero.

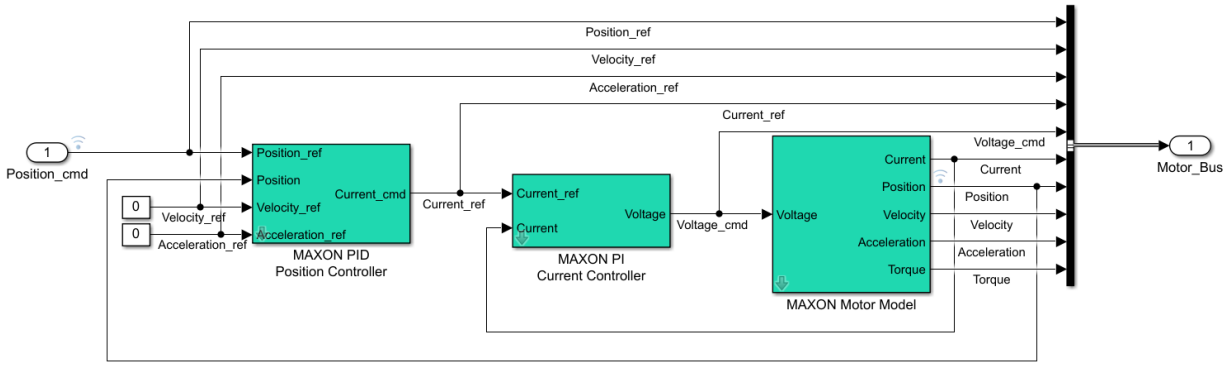

Fig. 8 Closed-loop actuator model

5. Actuator Controller Design

The actuator controller was tuned and tested using the Maxon EPOS Studio software, and control was implemented using a Maxon EPOS4 70/15 position controller. A DC power supply rated to 20 A at 30 V was used to power the experiment. In this experiment, the controller was tuned for a more aggressive response to minimize rise time while maintaining less than 15% overshoot for step commands. The tuned parameters for the PI current controller are given in Table 1, and the tuned parameters for the PID position controller are given in Table 2.

Table 1 Tuned parameters for current controller

Current controller parameters		
K_p	0.6163	V/A
K_i	2835.3	V/(A*s)
V_{max}	±30	V

Table 2 Tuned parameters for position controller

Position controller parameters		
K_p	6.3435	A/rad
K_i	70.2619	A/(rad*s)
K_d	0.0381	A*s/rad
FF_v	0.0096	A*s/rad
FF_a	1.2e-4	A*s^2/rad
I_{max}	±20	A

To demonstrate and evaluate the performance of the actuator with tuned controller, the closed-loop response of the actuator prototype was recorded for a 10° step input command, as shown in Fig. 9. The closed-loop responses for all three test events are consistent with one another and demonstrate a rise time of 5 ms with a 13% overshoot and a settling time of 30 ms. This response exhibits a very fast rise time and is within the 15% overshoot design criteria. If further analysis indicates issues from the 30-ms settling time, the controller aggressiveness can be scaled back to improve settling time at the expense of rise time.

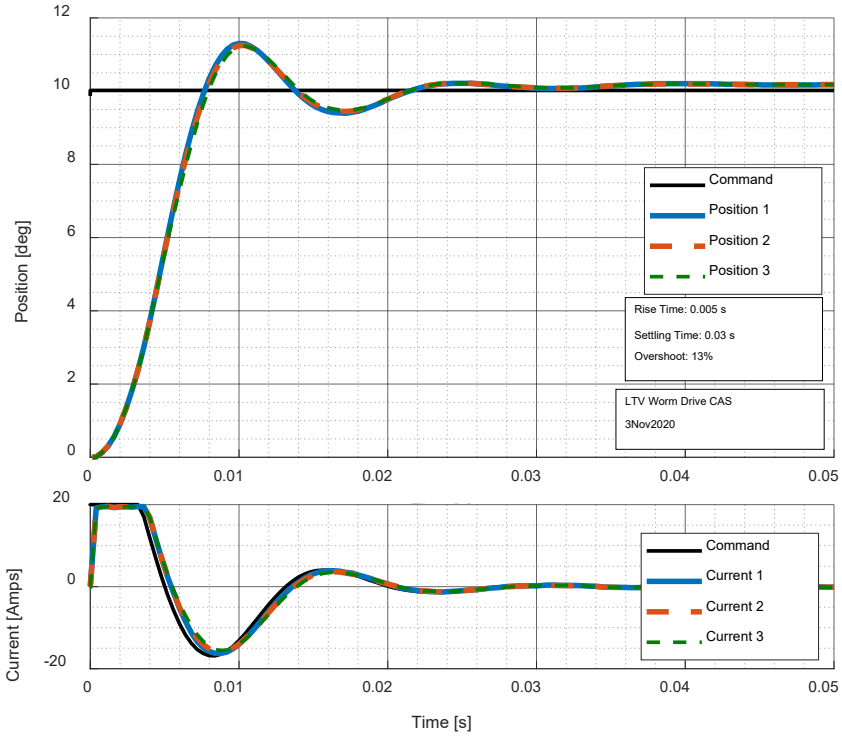

Fig. 9 Closed-loop actuator prototype experiment results for three 10° step input commands

6. Actuator Model Fit

The characteristic parameters of the Maxon EC-4pole motor given in Table 3 are used to populate the plant model to simulate the CAS response.[4] These motor-spec parameters are used as a starting point to fit the model to the performance of the motor–drivetrain assembly using a series of dynamic test events. As a starting point, μ_v is estimated using K_m and the no-load speed and current for the motor, given as n_0 and I_0, respectively:

$$\mu_v = \frac{K_m I_0}{n_0 \left(\frac{2\pi}{60}\right)}$$

Table 3 Characteristics of the brushless DC motor

Motor characteristic parameters (catalog)		
Terminal resistance, R	0.361	ohms
Terminal inductance, L	7.1e-5	H
Torque constant, K_m	0.0105	Nm/A
Electrical constant, K_e	0.0105	sV/rad
Rotational inertia, J	5.54e-7	kg/m^2
No-load speed, n_0	16,300	rad/s
No-load current, I_0	0.218	A
Viscous friction, μ_v	1.341e-6	Nm/(rad/s)

The closed-loop actuator model presented in Fig. 8 is populated with the tuned controller parameters and catalog motor characteristic parameters from Tables 1–3. The simulated response of the model with these original plant parameters is plotted in Fig. 10 as a green line. This modeled response does not agree well with the experiment (plotted in blue).

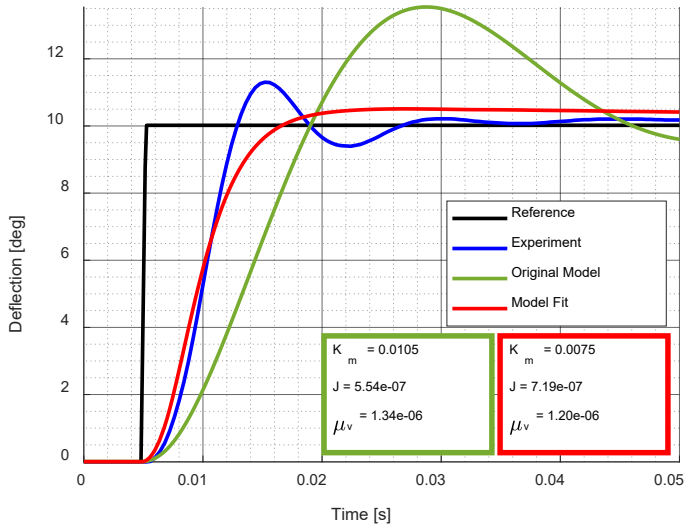

Fig. 10 Comparison of step response from closed-loop actuator model and experiment

A parameter estimation routine was used to adjust the K_m, J, and μ_v parameters in the motor model to better fit the model to the observed response in experiment. The simulated response of the model fit is plotted in red, with the parameter changes improving the fit of the model to the data significantly. These parameter fit values are given in Table 4. However, given that the motor model is defined using parameters based on physical properties, arbitrary adjustment of parameter values to improve the model fit points to shortcomings in the model itself. Future research

will look toward improving this physics-based motor model to better represent observed behavior.

Table 4 Parameter fit values for motor model

Motor characteristic parameters (fitted)		
Torque constant, K_m	0.0075	Nm/A
Rotational inertia, J	7.19e-7	kg/m2
Viscous friction, μ_v	1.2e-6	Nm/(rad/s)

7. Actuator Second Order Model Fit

In addition to more-complex, physics-based dynamic models, the closed-loop actuator response can be represented as a generic second-order ODE system parameterized by a natural frequency, ω_n, and a damping ratio, ζ. Defining a state vector, $\boldsymbol{x} = \left[\delta, \dot{\delta}\right]^T$, where δ is the position of the actuator and $\dot{\delta}$ is the actuator rate, this second-order system can then be expressed in state space as

$$\dot{\boldsymbol{x}} = \mathbf{A}\boldsymbol{x} + \mathbf{B}u(t)$$

$$\boldsymbol{y} = \boldsymbol{C}\boldsymbol{x}$$

where $u(t)$ is the input, and the system matrix, $\mathbf{A}$, input matrix, $\mathbf{B}$, and output matrix, $\mathbf{C}$, are defined as

$$\mathbf{A} = \begin{bmatrix} 0 & 1 \\ -\omega_n^2 & -2\omega_n\zeta \end{bmatrix}$$

$$\mathbf{B} = \begin{bmatrix} 0 \\ \omega_n^2 \end{bmatrix}$$

$$\mathbf{C} = [1 \quad 0]$$

A second-order actuator model of this form is shown in Fig. 11, which has been augmented by a time-delay parameter, t_d. A parameter estimation routine was used to identify a set of ω_n, ζ, t_d, which approximate the experimental system response using this second-order model. The routine identified a system with $\omega_n = 462$ rad/s, $\zeta = 0.54$, and $t_d = 0.002$ s as the best fit for the dynamic behavior. A comparison of the experiment response to this model fit is shown in Fig. 12.

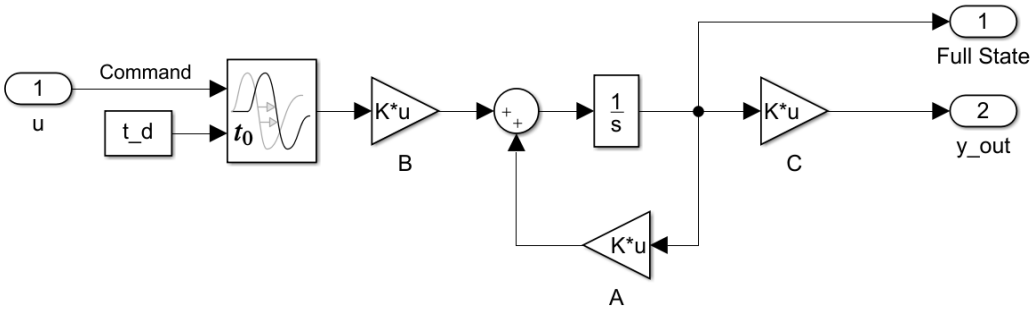

Fig. 11 Second-order ODE model for actuator

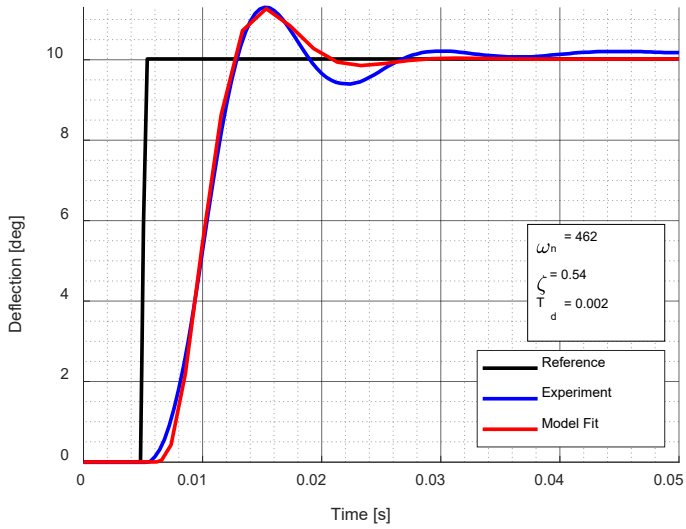

Fig. 12 Step response of experiment and second-order ODE model fit

In general, a damping ratio between 0.6 and 0.8 is usually targeted to provide a reasonable compromise between rise time and settling time, so this response is slightly underdamped to give a faster rise time. If further testing indicates the settling time is too large, this controller can be retuned to target a slower rise time in order to improve the settling time of the response.

Based on this model fit, the closed-loop actuator bandwidth can be estimated using the values of ω_n and ζ, as shown[5]:

$$\omega_{BW} = \omega_n \sqrt{(1 - 2\zeta^2) + \sqrt{4\zeta^4 - 4\zeta^2 + 2}}$$

Using this equation, the ω_{BW} is estimated at 566 rad/s, which is well above the design goal of 300 rad/s for the transient response of the of the actuator, based on the flight control design. This ω_{BW} value is for the unloaded actuator, however, and the system response is expected to slow when under in-flight loads. Future research

will analyze and quantify the actuator response while under expected flight loads, but the significant margin between the demonstrated unloaded performance and the bandwidth requirement generates confidence this actuator prototype will prove a viable option.

8. Summary and Conclusion

An actuator prototype design for a fin-controlled projectile was presented with descriptions of the mechanical design and the control-system architecture. The tuned control-system parameters were given, and results from bench-level experiments demonstrating the closed-loop dynamic response were presented and discussed. Models fitted to the experiment response data were used to characterize the dynamic behavior, and show the actuator met bandwidth requirements for these unloaded experiments.

Future research will focus on 1) improving the physics-based dynamic model of the actuator to better represent the observed response, and 2) developing test fixtures to explore the actuator response/performance when under expected in-flight aerodynamic loads.

9. References

1. Bryson J, Vasile J, Gruenwald B, Fresconi F. Control surface design analysis and actuation requirements development for munitions. Proceedings of the AIAA SciTech Forum; 2020 Jan 6–10; Orlando, FL. AIAA SciTech Paper No: 2020–0020.

2. Vasile J, Bryson J, Sahu J, Paul J, Gruenwald B. Aerodynamic dataset generation of a long-range projectile. DEVCOM Army Research Laboratory; Aug 2020. Report No.: ARL-TR-9019.

3. Maxon Group. Maxon EPOS4 positioning controllers application notes, edition 2019-11. DocID: rel8760.

4. Maxon Group. Maxon product catalog. 2020 Apr. p. 247.

5. Nise NS. Control systems engineering. 3rd edition. John Wiley & Sons; 2000.

List of Symbols, Abbreviations, and Acronyms

μ_v	viscous friction
ζ	damping ratio
δ	actuator position
$\dot{\delta}$	actuator rate
ARL	Army Research Laboratory
CAS	control actuation system
D	filtered derivative gain
DC	direct current
DEVCOM	US Army Combat Capabilities Development Command
FF_a	feed-forward acceleration
FF_v	feed-forward velocity
I_0	no-load current
I_{max}	maximum current
J	rotational inertia
K_e	electrical constant
K_i	integral gain
K_m	motor torque constant
K_p	proportional gain
L	winding inductance
LRPF	long-range precision fire
LTV	Laboratory Technology Vehicle
n_0	no-load speed
ODE	ordinary differential equation
PI	proportional–integral
PID	proportional–integral–derivative
PN	part number
QT-CAS	Quad Tail Control Actuation System
R	winding resistance

t_d	time-delay parameter
V_{max}	maximum voltage
ω_{BW}	closed-loop actuator bandwidth
ω_n	natural frequency

1 (PDF) DEFENSE TECHNICAL INFORMATION CTR DTIC OCA

1 (PDF) DEVCOM ARL FCDD RLD DCI TECH LIB

19 (PDF) DEVCOM ARL FCDD RLW A F E FRESCONI FCDD RLW LE J BRYSON B BURCHETT I CELMINS B C GRUENWALD J DESPIRITO L FAIRFAX L STROHM J PAUL J D VASILE FCDD RLW L T SHEPPARD W OBERLE FCDD RLW LB N TRIVEDI FCDD RLW LC J SADLER FCDD RLW LF M ILG B TOPPER D EVERSON FCDD RLW LH T EHLERS M MINNICINO